Dynamics of molecular reactions in solids: Photodissociation of F2 in crystalline Ar

R. Alimi, R. B. Gerber, and V. A. Apkarian

Citation: J. Chem. Phys. **92**, 3551 (1990); doi: 10.1063/1.457864
View online: http://dx.doi.org/10.1063/1.457864
View Table of Contents: http://jcp.aip.org/resource/1/JCPSA6/v92/i6
Published by the American Institute of Physics.

Dynamics of molecular reactions in solids: Photodissociation of F_2 in crystalline Ar

R. Alimi and R. B. Gerber[a)]
Department of Physical Chemistry and the Fritz Haber Research Center for Molecular Dynamics, The Hebrew University of Jerusalem, Jerusalem 91904, Israel

V. A. Apkarian
Department of Chemistry, University of California, Irvine, California 92717

(Received 16 October 1989; accepted 24 November 1989)

Classical molecular dynamics simulations of F_2 photodissociation in a host Ar crystal are presented. At temperature $T = 12$ K, the photodissociation yield shows a sharp threshold for an excess energy of ~ 0.6 eV, and it reaches nearly unity for excess energies above 2 eV. For a given excess energy, the quantum yield at 4 K is higher than a 12 K, and is predicted to remain finite even at 0 K. The transition state for photofragment exit from the reagent cage is found to be located in well-defined windows in the unit cell of the surrounding solid. The quantum yields (or photodissociation probabilities) are extremely high, especially at low T, in comparison with the values found in previous studies, e.g., for Cl_2 in Xe and in Ar. Indeed, for high excess energy the near-unit quantum yields indicate the virtual absence of an inhibiting cage effect on the reaction. The anomalous behavior of F_2 in Ar is attributed to the short effective range of the repulsive F/Ar interaction, which enables the F atom to exit the cage and migrate in the crystal. It is also due in part to the F/Ar attractive potential, which is found strong enough to focus and stabilize the migration of the F product in "channels" within the lattice, following photolysis. Classical trajectories show long-range migration of the product atoms, of the scale of 30 Å, following the initial impulse provided by the photodissociation. This is the first system for which such long-range impulse-induced migration was found. The results of the simulations are analyzed focusing on the role of the initial state of F_2 in the crystal, on the final sites occupied by the product atoms, and on the migration dynamics. Implications of the results for mechanisms of reactions in solids are discussed.

I. INTRODUCTION

The photodissociation of diatomics in ordered, crystalline van der Waals solids provides interesting fundamental models of condensed phase reaction dynamics. With this motivation we have initiated both experimental and theoretical investigations of photodissociation of molecular halogens and hydrogen halides in crystalline rare-gas solids.[1-5] The experimental studies to date have been limited to time-independent measurements, e.g., quantum yields as a function of wavelength, temperature and, most recently, pressure. The theoretical investigations have to date been limited to molecular dynamics simulations using gas-phase pair potentials, under the assumption of pairwise additivity. While a great deal of insight into the microscopic details of the photodissociation process is obtained from these simulations, only highly averaged quantities are compared with experiment. Even then, the comparisons should be made with great caution. As an example, in the case of photodissociation quantum yields it is important to note that the experiments measure the probability of "permanent" separation of atoms; while the simulations yield the probability of separation on a short time scale, typically 10 ps or so. Clearly, with the increased availability of convenient spectroscopic tools with subpicosecond resolution a direct comparison between experiment and theory in the time domain will become possible. However, in the absence of such data the theoretical simulations serve mainly as predictive and interpretive tools with only a loose queue from experiment.

The choice of the system for the present studies, F_2 in crystalline Ar, was motivated by several intriguing observations in recent experimental studies. In the first demonstrations of solid state XeF lasers in crystalline argon, it was clearly indicated that not only does F_2 photodissociate readily in these crystals of very high optical quality, but also that the F atoms migrate very large distances upon dissociation.[6,7] This finding has more recently been further supported by the observation of reversible shuttling of F atoms between Kr and Xe centers in multiply doped crystalline argon.[8] More rigorous quantification of the range of photoinduced mobility of F atoms in Ar has recently been obtained by recombination measurements.[9] In previous molecular dynamical simulations of photolysis of Cl_2[2] and of HI[3] in crystalline xenon, no such long-range migration of atoms could be observed. Neither was such an effect found in simulations of photodissociation of Cl_2 in large clusters of Ar.[10] The present simulations were initiated to provide microscopic insights into the observed special behavior of F_2 photodissociation. Indeed, an understanding of the special cases by simulations is essential for the building of general theories of reactive dynamics in ordered solids.

II. SYSTEM AND METHOD

The system used for the present simulations consists of one F_2 molecule embedded in a substitutional site of an fcc

[a)] Also: Department of Chemistry, University of California, Irvine, CA.

 0021-9606/90/063551-08$03.00

lattice of Ar atoms. The lattice is constructed as a cube of 365 atoms, with 194 static face atoms and 171 mobile bulk atoms (the central atom is replaced by F_2). The choice of this system, as opposed to a smaller cell with periodic boundary conditions, was made in order to clearly observe the expected long-range migration of dissociation products. Tests have established that with the model used, the behavior is converged with respect to size dependence.

The simulations are strictly classical. The positions for all 173 mobile atoms are updated by simultaneous integration of the Newtonian equations of motion, using the variable time step and variable order Adams–Moulton integrator. The forces on the mobile atoms are calculated from the gradient of the pairwise additive potential, using all 366 atoms in the force calculation. Prior to initiation of dissociation, the entire system is thermalized at the desired temperature. This is accomplished by initializing the dynamics from the configuration of the perfect crystal, by imparting random velocities selected from a Maxwell–Boltzmann distribution corresponding to a mean kinetic energy kT. The total energy of the system is followed periodically to check conservation. In typical runs of several picoseconds, the conservation in total energy of the system is better than 10 ppm.

The thermalized lattice is propagated in time for an additional 10–25 ps with F_2 in its ground-state potential. This file is then used for sampling of initial conditions for dissociation, by choosing configurations equally spaced in time from a given segment. The photodissociation process is simulated by suddenly switching the F_2 potential from its ground-state Morse form, to the excited exponentially repulsive form. The F_2 distance is adjusted to reproduce the desired photodissociation energy according to the Franck–Condon principle. The change in distance actually required is very small. The advantage of doing so is that it becomes possible to simulate photodissociation under monochromatic irradiation. It is important to note that no provisions are made of the dissipation of the excess energy initially introduced in the form of potential energy on the repulsive F–F surface. Thus the system will thermalize at a final temperature given by

$$T_f = T_i + \frac{2}{3k}\frac{E_{\text{excess}}}{n}, \tag{1}$$

where k is the Boltzmann constant, n is the number of mobile atoms (173 in the present example), and E_{excess} is the potential energy above the dissociation limit of F_2.

Most of the simulations were carried out on a Cray-2 computer. Typically, 1 ps of simulation could be completed in 1 min of CPU time. For efficient vectorization of the code, it is useful to cast all pair potentials in the same analytical form. To this end we have used the Morse form:

$$V(r) = D_e\{\exp[2\beta(1 - r/r_e)] - 2w\exp[\beta(1 - r/r_e)]\} \tag{2}$$

in which w allows switching from the standard Morse to a strictly dissociative exponential potential ($w = 1$ or 0), D_e, β and r_e have the standard meaning of dissociation limit, steepness and potential minimum, respectively. The parameters were obtained by fitting the gas-phase pair potentials. The parameters for Ar–Ar, Ar–F and F–F in the $1\,^1\Sigma_g$ and $^1\Pi_u$ potentials, are collected in Table I, along with the references to the original sources.

In the case of the ground state $F_2\,(^1\Sigma_g)$ the Morse parameters are based on the experimental frequency and dissociation limit.[13] However, the repulsive $F_2\,(^1\Pi_u)$ state parameters are taken from the *ab initio* calculation of Cartwright and Hay.[14] We note that while the purely theoretical surfaces of Cartwright and Hay well reproduce the first continuum absorption profile of F_2, the dissociation energy of their ground surface is in error by $\sim$0.25 eV (see discussion in Ref. 14). Thus, while their repulsive surface is used here, care should be taken in comparing the excess energies of the theoretical simulations with experimental photon energies. We also note that, the same F–Ar potentials are used independent of the electronic state of F_2. Thus the $F_2\,(^1\Sigma_g)$–Ar potential is simulated strictly as a sum of pairwise additive atom–atom potentials. This is perhaps the most serious approximation made in the calculations. Such a potential is likely to overemphasize the anisotropy of the atom–molecule interaction. However, in the absence of a better known F_2–Ar potential, it is a useful approximation. Where the results may be affected by this assumption will be discussed later in the text.

III. RESULTS AND ANALYSIS

A. Initial state dynamics

The description of the initial state dynamics, namely the motions of the molecular F_2 in the crystalline lattice, are crucial to the interpretation of the photodissociation results. Chief among these considerations is the initial orientation, and hence the rotational degrees of freedom, of the molecule in its trap site. The final outcome of the photodissociation clearly depends on the initial orientation. Moreover, the motions in the initial state determine the statistical sampling for averaged final quantities such as dissociation quantum yields. Thus we provide analyses for the rotation, translation, and vibration of the substitutionally trapped F_2 in Ar.

The axes used in the simulations, together with a unit cell is provided in Fig. 1. The angle subtended between the F_2 internuclear axis and the z axis is designated by θ. The time evolution of θ for the initial 10 ps (with initial conditions, $\theta = 0$ at $t = 0$) is shown in Fig. 2 by the dotted line. θ oscillates between 0° and 60° several times before flipping to a new local minimum at 120°. The motion of the center of mass of the molecule is shown by the solid line in the same figure (Fig. 2). The center of mass rapidly leaves the center of interaction where it was initially placed, and remains eccen-

TABLE I. Potential parameters used in the calculations, see the text for the formula.

Atoms pair	D_e (eV)	β	r_e (Å)	W	Ref.
Ar–Ar	12.3×10^{-3}	6	3.76	1	11
Ar–F	12.1×10^{-3}	4.30	2.95	1	12
F–F ($^1\Sigma_g^+$)	1.60	4.27	1.41	1	13
F–F ($^1\Pi_u$)	2.80	3.62	1.41	0	14

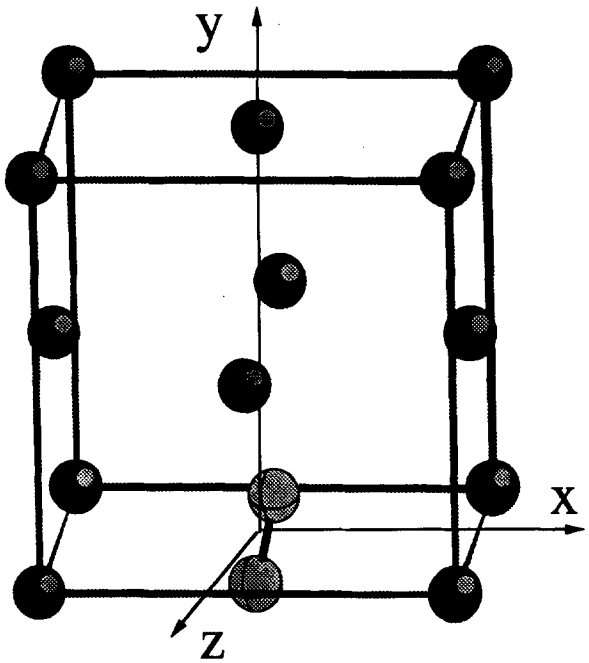

FIG. 1. Geometry of impurity molecule in an undistorted fcc Ar lattice (F_2 in gray). The angle θ in the text is the polar angle between the Y axis and the molecular axis.

tric, undergoing large amplitude motions of ~ 0.6 Å. There is a striking correlation between the molecular orientation and its center of mass. This can clearly be seen in Fig. 2, in which each undulation in θ appears accompanied by a similar motion in the c.m. The large angles are also accompanied by large eccentricity. The F_2 motion is quite free in the cage and fits the description of the classical rotation–translation coupling models.[15]

The time evolution of the F_2 internuclear separation is shown in Fig. 3 for a 1 ps segment of the thermalized system at 12 K. In addition to the high frequency F_2 vibrational motion, two observations are noteworthy: (a) the equilibrium internuclear separation of F_2 of 1.412 Å, has shifted to a shorter length, (b) the F_2 internuclear separation and its mean value (equilibrium separation) are modulated by a low frequency motion. The power spectrum of this motion obtained by Fourier transformation of $R_{F-F}(t)$, is shown in Fig. 4. Two transform limited sharp peaks, one at 890 cm^{-1}

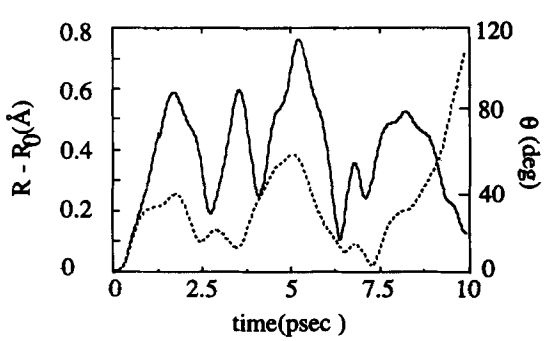

FIG. 2. Motion of the center of mass of F_2 (solid line, left y axis) and of θ (dashed line, right y axis) vs time (at $T = 12$ K).

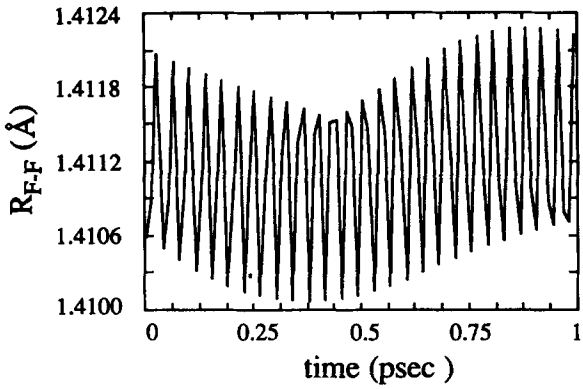

FIG. 3. Time dependence of the internuclear F_2 distance (at $T = 12$ K).

and another at 22.4 cm^{-1}, clearly stand out in the spectrum. They can clearly be identified as the F_2 internal vibration and the frequency of the motion of the molecular center of mass. Note that while the 22.4 cm^{-1} peak occurs in the bulk phonon frequency range, it is very strongly localized and therefore fits the description of a resonance mode. The slow modulation in Fig. 3 is due to this motion, which is verified by the observation of the same sharp spectral feature in the Fourier transform of the center-of-mass motion of Fig. 2. The frequency of the F_2 internal vibration in the lattice is not shifted significantly from the gas phase value. The absence of a "matrix shift" in this case is in accord with experiment,[16] and further supports the notion that F_2 is only very weakly coupled to the lattice. The internal motion is essentially pure and not coupled to the phonon bath as is also seen from the absence of any sidebands. This is very different from the case of HI in solid Xe in which case the entire phonon spectrum appears as a sideband on the internal vibrational peak at 2200 cm^{-1}.

In summary, F_2 is approximately a free rotor in the argon cage, and certainly an almost unperturbed oscillator. However, its rotational motion is strongly coupled to the translation of its center of mass whenever the F_2 "collides" with the cage walls. The most important (but in itself small) mechanical coupling of the internal F_2 modes is to the localized c.m. vibration of the F_2 with respect to the lattice. The

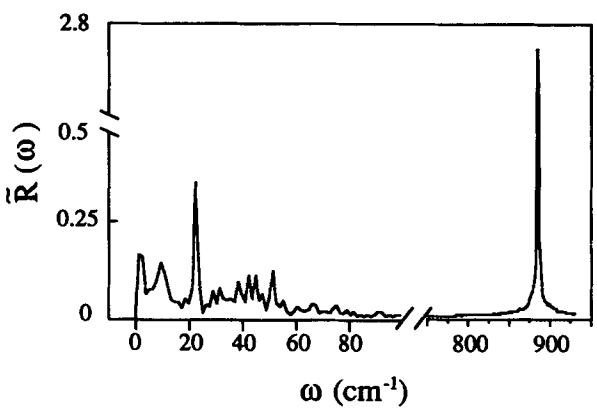

FIG. 4. Fourier transform of Fig. 3 (a longer run, about 25 ps was used for the calculation). Both the x and y axes were cut in order to show the two well separated regions of the spectrum.

coupling to the bulk lattice phonons is completely insignificant.

Similar studies were performed for the system thermalized to 4 K. The main difference in this case is that θ is now limited to values between $\pm$ 12°, and the molecular axis does not flip for simulation periods of $\sim$10 ps. At 4 K, the molecule librates in a local potential minimum. Jumps between such minima become rare events which may be mediated by rotational tunneling in the real system. Clearly, it is the description of these librational barriers that are strongly affected by the choice of the F_2–Ar potential. The very anisotropic potential used here may be responsible for the observation of the sharp transition between the rotation–translation coupled motion and the librational motion observed for a change in temperature from 12 to 4 K.

B. Photodissociation

Photodissociation studies were conducted at two different temperatures, 12 and 4 K, and for five different excess energies (four in the case of 4 K studies). For each energy, fifty trajectories were sampled. The emphasis in presenting the results will be on the main qualitative features. Thus, we will discuss the 12 K trajectories with some detail, and only describe the qualitative differences observed at 4 K. For initial conditions of the 12 K simulation, the segment between 7.26 and 9.66 ps of the initial state simulation shown in Fig. 2 was used. This guarantees that the sampling is from the full range of angles accessed by the molecule ($\theta = 0°$–$60°$) in its local minimum. Each trajectory was propagated until the F atoms (and the entire system) were thermalized. This typically occurred on the time scale of several picoseconds. The statistics on these trajectories is collected in Tables II and III, for the 12 and 4 K simulations, respectively. The fraction of runs that leads to separation of the F atoms by more than one lattice site gives the photodissociation quantum yields ϕ. These are plotted in Fig. 5 as a function of excess energy. The error bars in the figure are due to the limited number of the trajectories used. Under the assumption of random sampling, the error bars scale with $n^{1/2}$ where n is the number of trajectories. Since the randomness of the sampling is not guaranteed, the indicated error bars should be regarded as lower bounds for the true uncertainty. In addition to ϕ, important observables for understanding the process are the distribution of the F atoms among the possible final sites in the crystal, and the probabilities of symmetric and asymmetric cage exit events (i.e., probability that both F atoms leave or only one of the F atoms leaves the cage). All these properties are listed as a function of the excess photodissociation energy in Tables II and III (for $T = 12$ K and $T = 4$ K, respectively).

TABLE II. Summarized results of 50 trajectories each at 12 K. Φ is the quantum dissociation yield.

Excess energy (eV)	Φ	Final populated sites			Symmetric exit	
		T_d	O_h	Substitutional	Yes	No
0.5	0	0	0	0	0	0
0.75	12%	0	50%	50%	0	100%
1.0	55%	0	75%	25%	75%	25%
2.0	90%	0	73%	25%	90%	10%
2.8	98%	0	82%	10%	100%	0

TABLE III. Same as Table II for $T = 4$ K.

Excess energy (eV)	Φ	Final populated sites			Symmetric exit	
		T_d	O_h	Substitutional	Yes	No
0.5	6%	0	66%	34%	30%	70%
0.75	40%	0	63%	37%	33%	67%
1.0	75%	0	80%	20%	90%	10%
2.0	86%	0	70%	30%	93%	7%

1. Dissociation yields

At 12 K, no dissociation is observed for an excess energy of 0.5 eV or less. The dissociation probability sharply increases with excess energy, as illustrated in Fig. 5, from which a threshold energy of $\sim$0.6 eV, i.e., 0.3 eV per F atom, can be estimated. This closely coincides with the barrier to passage of F atoms through the three atom faces of a perfectly rigid argon solid which we estimated from the calculated energy contours. The dissociation probability rises rapidly beyond the threshold and is nearly unity at excess energies above 2 eV.

At an excess energy of 2.8 eV, only one trajectory terminates with both F atoms at the original site. A closer investigation of this trajectory revealed that it was due to recombination after symmetric exit. This trajectory is illustrated in Fig. 6 in which a two-dimensional plot of the time-ordered sequence of the F atom cartesian coordinates are shown (upper panel). The time evolution of the kinetic energy in each F atom for the same trajectory is shown in the lower panel of Fig. 6. Both F atoms initially accelerate in the potential field and travel ballistically for $\sim$3 Å without being deflected. During this state, the kinetic energy of the pair reaches the full value of the initial excess energy. After an initial deflec-

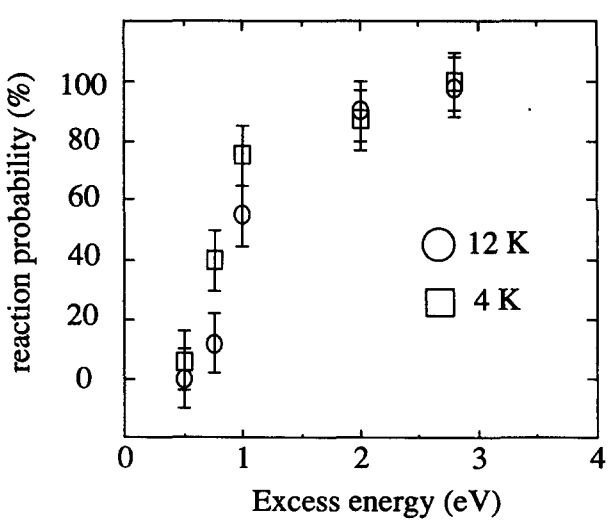

FIG. 5. Probability of exit from reaction cage as a function of the excess photodissociation energy for two temperatures.

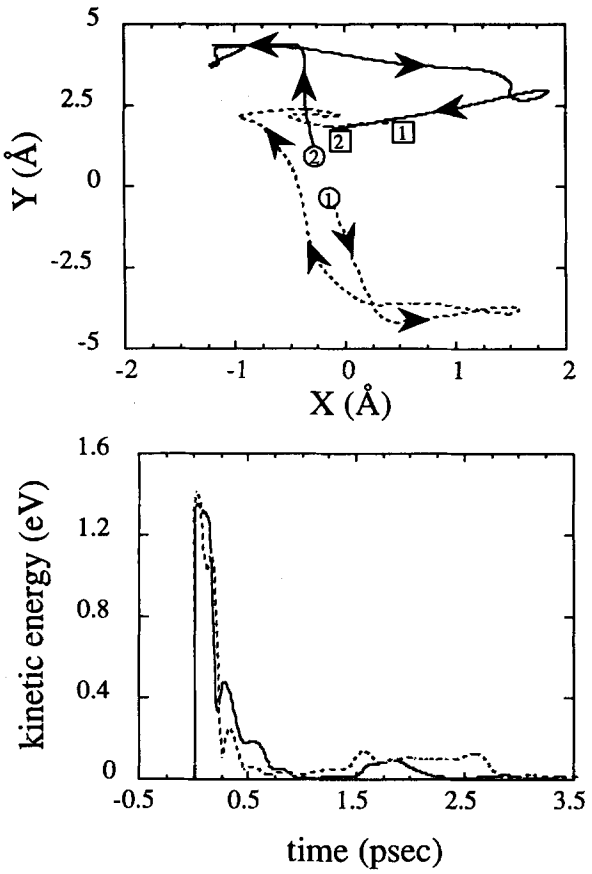

FIG. 6. Nonreactive trajectory for an excess energy of 2.8 eV (at $T = 12$ K). (a) shows the projection on the xy plane of the paths followed by the fragments 1 and 2. Initial positions are denoted by the circles, final positions (after 3.5 ps) are denoted by squares. The arrows indicate the direction of the motion. 6(b) shows the time dependence of the kinetic energy of the fragments (dashed line and plain line for fragments 1 and 2, respectively).

tion, atom 1 undergoes a head-on collision, and the trajectory nearly retraces itself. Most of the kinetic energy is lost with this head-on collision, 0.25 ps into the flight; and the atom returns to its original site with ~0.15 eV of excess energy. The journey of the second atom is more extensive. It visits four different sites and returns to the original after a flight time of ~2.5 ps. Atom 2 reenters the original site nearly completely thermalized. The kinetic energy loss in this case occurs in several hard collisions—collisions upon which more than 50% of the atomic kinetic energy is lost. However, it is important to note that these secondary collisions produce mainly curvilinear trajectories, as opposed to sharp corners. These collisions are always multiple in nature as opposed to single collision events followed by rectilinear free flight. The first near head-on collision in this case can also be identified to occur after ~0.2 ps of flight. Finally, it is important to note that this recombination is not an artifact of the rigid lattice wall—while the atoms visit many sites, they never reach the edge of the solid.

The mechanism illustrated by this trajectory, namely geminate recombination due to hot atom random flights, is the mechanism responsible for the fact that the dissociation probabilities are less than unity even at high energies. It should be stressed that "geminate," short time scale recombination is a far more probable event in other systems, e.g., Cl_2 in Xe[2] and HI in Xe[1]. In those cases, however, the geminate recombination events are due to the photofragments being contained by the cage walls. The present case is unique in showing recombination after a long-distance excursion of the products outside the cage has taken place. The probability for such recombination following long-range excursion of the products is small at high excess energy, but this effect together with the near unity Φ show how unique the cage effect is for F migration in Ar. In fact, it can be said that at high excess energy there is *essentially no cage effect in this system inhibiting the photodissociation process.* We will return to discuss this highly unusual behavior.

While initially not suspected, at 4 K the dissociation probabilities are larger than those at 12 K. The main clue to the causes of this effect is the strong correlation between initial orientation of F_2 relative to the cage, and the final separation between F atoms. Despite the limited statistics, sorting of the 12 K, 1 eV trajectories (in which 50% lead to dissociation) according to initial angles, clearly indicates that there are two reaction cones in a quadrant of the unit cell. These reaction cones are illustrated in Fig. 7. The first cone, subtends a rather acute solid angle near $\theta = 10°$ and leads to an indirect passage to the second nearest interstitial O_h site (at $a/2$, a, 0 in the unit cell of Fig. 1). The second cone is more obtuse, and leads to the first nearest interstitial O_h site (at $a/2$, $a/2$, $a/2$ in the unit cell of Fig. 1) via the C_3 barrier. At 12 K, as was discussed above, all of these angles can be realized, including the regions of nonreactivity. At 4 K, the molecule is rather tightly aligned in the first reactive cone. As a result, the sampling at 4 K leads to a large fraction of reactive trajectories. Clearly, the definition of these cones of reactivity become sharp only at low energy. At high energies all angles lead to dissociation. For a classical system, the dissociation probability of 0 would be predicted at 0 K, since

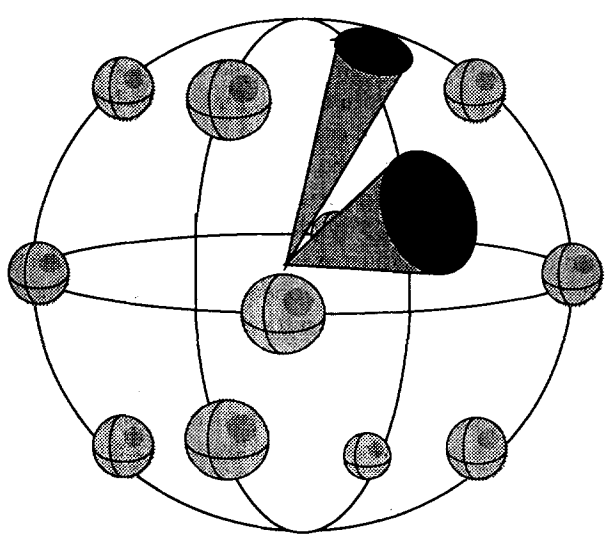

FIG. 7. The twelve atoms of the reaction cage (= one fcc unit cell) lie on a sphere the center of which is originally occupied by the F_2 center of mass. The two cones show the initial orientations of the molecule that result in separation of products.

the molecule would be locked in place at $\theta = 0°$. However, due to the librational zero-point energy, in a quantum mechanical system a perfect orientation is not possible. From the librational frequency of F_2, with the assumption of a harmonic well, the F_2 zero-point amplitude in the θ motion can be estimated at 11.5°. This is very near the average value of θ for the classical system at 4 K. It can therefore be safely predicted that even at absolute zero the F_2 dissociation cannot be eliminated; moreover, the dissociation probability at 0 K should be very similar to the classical results obtained at 4 K.

Finally, we stress again what may be the most interesting feature of the results both at 4 K and at 12 K: The quantum yield for separation of the F atoms at high energy is near unity. *This means that the surrounding solvent is so "porous" for the products that there is no inhibiting cage effect on the photodissociation.* This behavior is due primarily to the fact that the F/Ar cross section or effective interaction range at high energies is small. This refers, of course, to the repulsive part of the potential. On the other hand, the F–Ar attraction is substantial (of the order of the Ar–Ar well-depth), and this tends to stabilize the "out of cage" sites of the F products, once they exit the cage. Finally, the F/Ar mass ratio, while favorable for energy transfer from F to the lattice, leads to enhance dissociation yields. Unlike, e.g., H in a Xe lattice, the F atom can "push" the cage walls.

2. Final sites

As can be seen from the statistics in Tables II and III, no atoms are found in final T_d sites. Sojourn at T_d sites is, however, mandated in all dissociating trajectories. T_d sites are therefore dynamically metastable. In several trajectories visitations at T_d sites with nearly complete thermalization of the visiting atoms are seen. However, in none could successful retention be observed. An example of such a trajectory, chosen from the 1 eV runs, is shown in Fig. 8.

In the upper panel of Fig. 8, the distances of the F atoms from their initial positions are shown as a function of time. The time evolution of their kinetic energies is shown in the lower panel of Fig. 8. In this example, the dissociation is asymmetric: atom 2 stays in the original cage while atom 1 exists. After an initial hard collision and several subsequent deflecting bounces, atom 1 burrows itself in a distorted T_d site. It stays in this site for a period of nearly 0.5 ps (indicated by an arrow in the trajectory plot). The atom is fully thermalized during this sojourn as can be seen from the kinetic energy plot. The site, however, opens up by thermal fluctuations and the F atom hops out into the more stable, adjacent O_h site. The signature of this process is quite clearly seen in the kinetic energy plot. In the process of the hop-out, the F atom gains kinetic energy, the equivalent of the potential difference between the two sites, and loses it again to the new site, to be permanently trapped there. This appears as a kinetic energy burst, which is indicated by the arrow in the lower panel of Fig. 8.

Most, but not all, of the atoms that exit the cage terminate in interstitial O_h sites. At high excess energies, 2 and 2.8 eV trajectories, some of the atoms are found in newly created substitutional sites. A close inspection of Tables II and III

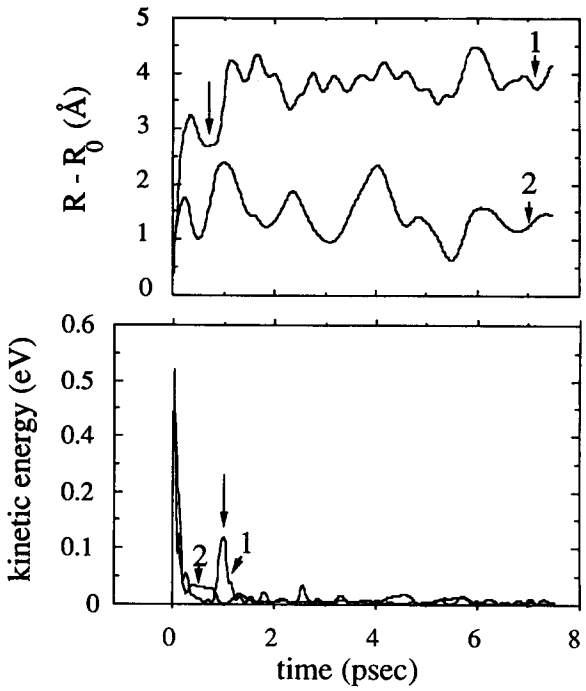

FIG. 8. Reactive asymmetric trajectory (excess energy = 1.0 eV, $T = 12$ K). (a) shows the time dependence of the distance of each fragment (noted 1 and 2) from its initial position. Fragment 1 leaves the cage and reaches an interstitial O_h site, after passing through a T_d site (shown by the first arrow). Fragment 2 stays in the original substitutional site. In (b) the kinetic energy of fragment 1 is plotted, where the arrow indicates the exit from the intermediate T_d site.

reveals this. At 12 K, and for a dissociation energy of 2.8 eV, all reactions are symmetric, yet 10% are found in substitutional sites—all of these are created by the hot atom. An even larger fraction of the dissociating trajectories at 2 eV leads to the creation of new substitutional sites. In all cases, the new site is either a nearest neighbor or a second-nearest neighbor of the original site of the isolation of the molecule. Thus, the new sites are created at the expense of blocking the vacancy left behind upon cage exit of the atoms. This also explains the fact that at 2.8 eV, a smaller fraction of the trajectories create substitutional sites, since typically they trap far away from the vacancy left behind. At energies below 1 eV, no new substitutional sites are observed. Thus, the probability of trapping of fragments in final substitutional sites peaks at an excess energy at which the F atoms possess sufficient momentum to dislodge Ar atoms, yet not enough energy to migrate too far from the original trapping site.

The different final sites could, in principle, be identified experimentally by their local frequencies. The power spectra of the F atom motions in the O_h site indicate a local mode frequency of $\sim 70\ cm^{-1}$; while for the substitutional sites a broad band between 30 and 40 cm^{-1} is observed. For the F–Ar Morse potential used in these simulations, a vibrational frequency of $\sim 33\ cm^{-1}$ can be calculated. Therefore, the observed vibrational frequencies in the substitutional sites simply reflect the fact that the site is very large and that the F atom essentially experiences at each instant a force field due to a single Ar atom. In the interstitial site, the pairwise additive potentials are reinforced to yield a nearly harmonic well

with a second-order gradient twice as steep as that of the isolated pair.

3. Long-range migration

The totals in the final site statistics presented in Table II do not add up to 100%. The missing atoms were those that exited the simulated solid slab. One such trajectory was observed at 2 eV and four at 2.8 eV. In all cases the trajectories show the same pattern—a wiggly motion along a lattice diagonal such as the 110 direction, without any sidesteps. An example is shown in Fig. 9, the evolution of the kinetic energy of the F atom for the same trajectory is shown in Fig. 10. Only one quadrant of the simulated lattice is shown in Fig. 9, with the argon atoms frozen in their equilibrium positions, while a time sequence of the F atom positions is shown. The hot atom is channeled by the lattice through a path that can be described as follows: It passes from diagonally arranged O_h sites in a single plane, entering each through the C_3 faces of the connecting T_d sites. To accomplish this most efficiently, the path bends around corners and never centers completely in the O_h site. Note that the only head-on collision suffered in this trajectory where the path retraces itself, is the collision with the rigid face atom. All other bends in the path can be described as deflection, or more appropriately, redirection of the F atom by the soft lattice. The entire process from dissociation to exit of the solid slab modeled in the computation lasts less than 1 ps, and clearly at the point of exit the atom contains sufficient energy to continue this path. Given the very regular pattern of kinetic energy loss per travel length (depicted in Fig. 10) it can be clearly deduced that the atom would have continued in this path for at least two more lattice sites, for a total travel length of ~30 Å! A linear fit to the time evolution of the kinetic energy yields 0.05 eV/Å as the energy loss per penetration length. It should again be noted that the main loss occurs in the initial stage of the trajectory, during the collisions that direct the hot atom into the channel. Once in the channel the atom follows a curvilinear path very efficiently tracing the channel.

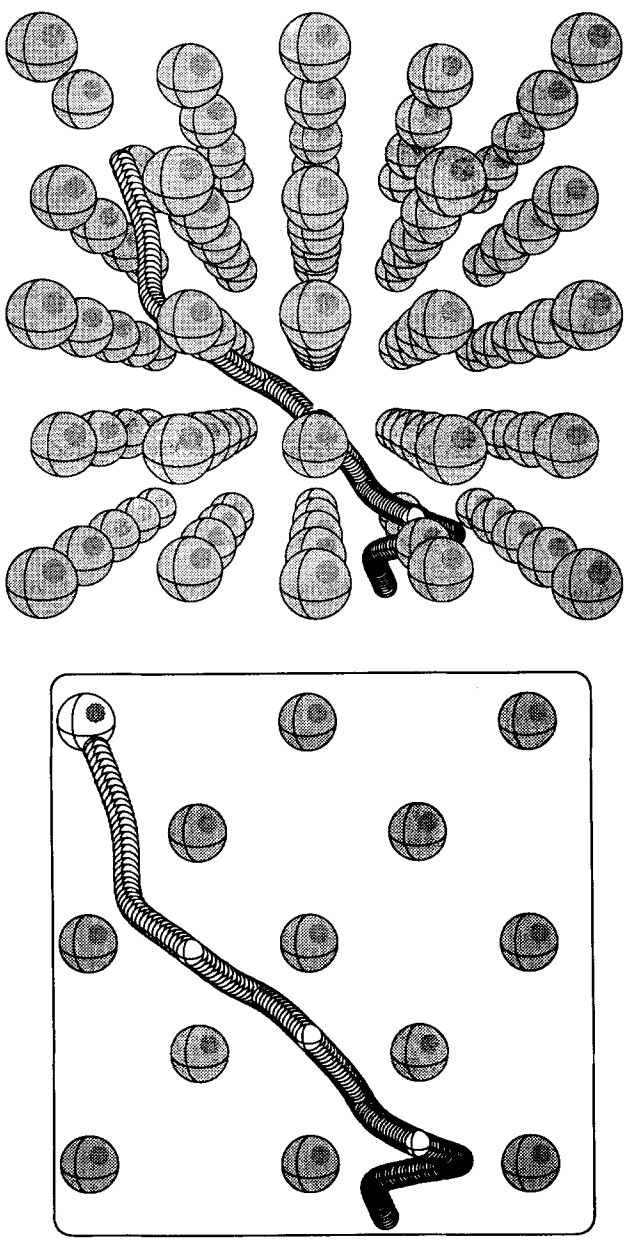

FIG. 9. Two different views of the motion of a F fragment traveling through the whole sample and finally leaving it ($E = 2.8$ eV, $T = 12$ K). The path goes from the upper left corner to the bottom right one. (a) and (b) are 3D views, the first one shows all the lattice atoms surrounding the path, while in the second, only the plane (yz) in which the F motion occurs is represented.

The fascinating aspect of this trajectory, beside the fact that it leads to very long-range migration of atoms, is that the motion of the hot atom in the randomly fluctuating lattice seems almost coherent. In fact, a characteristic of all of the observed trajectories is that after one hard collision, the rest of the interactions are soft and as a general rule many-body in nature. This is a very different situation than the H–Xe or Cl–Xe collisions observed in the photodissociation studies of HI and Cl_2. The F atoms in the present arrangement seem to be guided by the lattice rather than by its individual constituent atoms. While this is most evident in the wiggly trajectory of the long-range traveller, it is also clear in all inspected trajectories where instead of sharp angles, the trajectories are mostly comprised of curves. The reason for the remarkable channeling migration of F in Ar is twofold: First, the

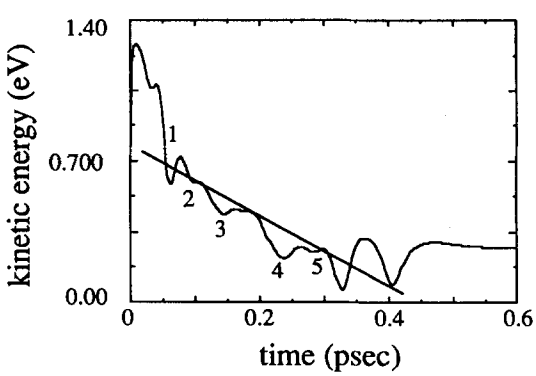

FIG. 10. Time dependence of the kinetic energy of the fragment shown in Fig. 9. The straight line fits the average loss of energy during the motion through the exit channel.

repulsive part of the F–Ar potential is short range, leaving sufficient room in the crystal for classically allowed channels of motion at the energy available to the F atom. Second, the attractive part of the F–Ar interaction is relatively strong and occurs at a short interatomic distance. The attractive potential focuses and stabilizes the motion of the F atom in the channels. It would be expected that the lattice will cease to be as elastic at high collision energy and tentative evidence to support it is already available. Hard F/Ar collisions and extensive energy transfer are then expected. It is therefore believed that the observed channeling will vanish at very high excess energies leading to a substantial slowing down of the F atom.

CONCLUSIONS

The photodissociation of F_2 is qualitatively different from all the systems previously studied theoretically. The main points of difference are:

(1) The photodissociation yield at high excess energies is extremely high approaching unity. The solid solvent then acts as a highly porous medium that does not exert an inhibiting cage effect;

(2) F_2 photodissociates in Ar with a permanent separation of the products at all temperatures, even at 0 K.

(3) Long-range ($\sim$30 Å) migration of the F atom after the photodissociation impulse often occurs.

(4) Geminate recombination of the F atom, when it occurs, typically involves long-range excursions of the F atoms before the recombination.

The immediate cage exit of the F atoms occurs by a ballistic motion, which yields a rather sharp threshold for dissociation probabilities as a function of excess energy. This behavior is somewhat similar to the Cl_2 photodissociation in Xe.

Both the temperature and excess energy of dissociation quantum yields are strongly determined by the initial F_2 orientation in the cage. The motion of F_2 in the argon cage fits rather perfectly the descriptions of the classical rotation–translation coupled system.

The photodissociation products, the hot F atoms, take circuitious interstitial paths in the argon lattice always terminating in an O_h trap site. These paths are characteristically composed of soft curves guided by the fluctuating lattice.

The fate of the fragment atoms strongly depends on their initial kinetic energies, as well as the temperature of the solid. For example, the probability for creating new substitutional sites peaks at 2 eV in the 12 K lattice, while it is not at all observed in the 4 K solid.

F_2/Ar is the first system in which very long-range photodissociation-induced migration of atoms at moderate energies is observed. These trajectories indicate that the motion is quite coherent and guided by the fluctuating lattice. This migration should, however, not be identified with thermal diffusion, although it is assisted by the lattice vibrations.

The photodissociation of F_2 in solid argon has been recently studied experimentally. The results of the experiments are in good qualitative agreement with most of the aspects observed in the present simulations. These include the observation of facile dissociation at all accessible energies, a sharp threshold in the photodissociation quantum yields as a function of excess energy, trapping of F atoms in O_h sites with agreement between the experimentally observed local frequency of the F atom and that calculated here, and finally long-range migration of the F atoms which has previously been observed and has more recently been quantified. These experimental results were obtained in a series of studies by several different techniques, an understanding of the details of which are essential for a meaningful comparison with theory. The detailed comparisons are taken up in the experimental papers.

ACKNOWLEDGMENTS

The support of this work by the U.S. Air Force Astronautics Laboratory under Contract No. F04611-87-K-0024 (to V.A.A.), is gratefully acknowledged. This research was supported in part by a grant from the Division of Basic Research of the Israel Academy of Sciences (R.B.G.). The Fritz Haber Research Center is supported by the Minerva Gesellschaft für die Forschung, mbH, Munich, BRD. Partial support from the Institute of Surface and Interface Science at U.C. Irvine, is also gratefully acknowledged.

[1] R. Alimi, R. B. Gerber, and V. A. Apkarian, J. Chem. Phys. **89**, 174 (1988).
[2] R. Alimi, A. Brokman, and R. B. Gerber, J. Chem. Phys. **91**, 1611 (1989).
[3] R. Alimi, R. B. Gerber, and V. A. Apkarian, Chem. Phys. Lett. **158**, 257 (1989).
[4] W. Lawrence, F. Okada, and V. A. Apkarian, Chem. Phys. Lett. **150**, 339 (1988).
[5] M. E. Fajardo, R. Withnall, J. Feld, F. Okada, W. Lawrence, L. Wiedeman, and V. A. Apkarian, Laser Chem. **9**, 1 (1988).
[6] N. Schwentner and V. A. Apkarian, Chem. Phys. Lett. **154**, 413 (1989).
[7] A. I. Katz, J. Feld, and V. A. Apkarian, Opt. Lett. **14**, 441 (1989).
[8] H. Kunttu, J. Feld, and V. A. Apkarian (submitted).
[9] J. Feld and V. A. Apkarian (manuscript in preparation).
[10] R. Alimi, R. B. Gerber, and A. Brokman, in *Stoichasticity and Intramolecular Redistribution of Energy*, edited by R. Lefebvre and S. Mukamel (Reidel, Dordrecht, 1987).
[11] U. Buck, Adv. Chem. Phys. **30**, 314 (1976).
[12] C. H. Becker, P. Casacecchia, and Y. T. Lee, J. Chem. Phys. **70**, 2986 (1979).
[13] K. P. Huber and G. Herzberg, *Constants of Diatomic Molecules* (Van Nostrand, New York, 1979).
[14] D. C. Cartwright and J. Hay, J. Chem. Phys. **70**, 3191 (1979).
[15] See, for example, H. Friedman and S. Kimel, J. Chem. Phys. **43**, 3925 (1965).